

Temporal Super-resolution for Wire Position Estimation in Electric Discharge Machines

Mansour, Hassan; Boufounos, Petros T.

TR2022-124 October 12, 2022

Abstract

We present a technique for achieving ultra-high temporal super resolution of the position of the cutting wire in electric discharge machines from low frame rate video. Our approach models the video of the vibrating wire as a frequency sparse signal and formulates a joint-sparsity recovery problem to determine the vibration frequency as well as reconstruct the high frame rate video. The proposed method is capable of reconstructing the high frame rate video at 5000 x super resolution rate. We demonstrate the performance of our method using simulated data mimicking the acquisition setup and wire vibrations in realistic EDM settings.

Mitsubishi Electric Research Laboratories

© 2022 MERL. This work may not be copied or reproduced in whole or in part for any commercial purpose. Permission to copy in whole or in part without payment of fee is granted for nonprofit educational and research purposes provided that all such whole or partial copies include the following: a notice that such copying is by permission of Mitsubishi Electric Research Laboratories, Inc.; an acknowledgment of the authors and individual contributions to the work; and all applicable portions of the copyright notice. Copying, reproduction, or republishing for any other purpose shall require a license with payment of fee to Mitsubishi Electric Research Laboratories, Inc. All rights reserved.

Temporal Super-resolution for Wire Position Estimation in Electric Discharge Machines

Hassan Mansour, Petros Boufounos

March 1, 2021

Abstract

We present a technique for achieving ultra-high temporal super resolution of the position of the cutting wire in electric discharge machines from low frame rate video. Our approach models the video of the vibrating wire as a frequency sparse signal and formulates a joint-sparsity recovery problem to determine the vibration frequency as well as reconstruct the high frame rate video. The proposed method is capable of reconstructing the high frame rate video at $5000\times$ super resolution rate. We demonstrate the performance of our method using simulated data mimicking the acquisition setup and wire vibrations in realistic EDM settings.

1 Introduction

Knowledge of the exact position and shape of the cutting wire in electric discharge machines (EDM) is important for determining the tension in the wire and the quality of the cut. The vibration frequency of these wires generally ranges around 1 KHz, which would require a camera with at least 2000 frames per second (fps) acquisition rate to exactly localize the wire. Since such high speed cameras would add a significant cost to the equipment, we aim to use standard frame rate cameras along with time-coded illumination or aperture, and computation to recover the vibrating frequency and exact position of the wire.

We pose the problem of estimating the vibrating wire position as a temporal super resolution problem from low frame rate video. Let m be the number of video frames captured by the camera in one second, with corresponding duration of each frame $t_f := \frac{1}{m}$. We will employ a coded illumination pattern $\mathbf{a}_i \in \{0, 1\}^n$, for $i \in \{1 \dots m\}$, occupying a time segment of duration $s < t_f$ seconds. The duration of this code corresponds to the exposure/acquisition interval of the low-rate camera, over which the code is active. Typically, this interval is significantly lower than t_f in practice, as the camera requires some time to transmit the data and reset.

The pattern \mathbf{a}_i is active during that interval, strobing at uniform rate according to the code, i.e., each coefficient of the pattern is active for a time

interval $t_s = \frac{s}{n}$. The interval t_s also corresponds to the target temporal resolution time step of the super resolved video, i.e., we effectively assume the video is approximately constant over that interval. For simplicity, we assume that $t_f = cs, c \in \mathbb{N}$, is an integer multiple of the of the segment duration t_s . Consequently, the target super resolved video will have $N = cnm$ temporal samples for every m video frames captured by the camera, i.e., we are targeting a super resolution rate of $cn \times$ temporal upsampling.

The most closely related work on this topic appear in [1] and [2]. In [1], a streaming compressive sensing algorithm specifically tailored to the reconstruction of high speed video from low speed coded frames. Their approach uses a greedy reconstruction algorithm that allows causal on-line acquisition and reconstruction of the video, with a small, controllable, and guaranteed buffer delay and low computational cost. In [2], each pixel location of the video is considered an independent periodic frequency-sparse signal of unknown fundamental period, compressively acquired at the rate of the low-speed video sensor. A greedy reconstruction algorithm is also used in that work, combined with several computational heuristics to recover the high-speed time waveform of each pixel, and reconstruct the high-speed video from the acquired data. In this note, we employ a similar jointly-sparse signal model and find a frequency sparse signal that represents the high speed video. Contrary to the previous work, we set up a convex optimization problem using weighted $\ell_{2,1}$ minimization. We also develop a dimensionality reduction scheme that compresses the dimensionality of the optimization variable while maintaining the sparsity structure of the problem to make it computationally tractable.

2 Problem Formulation

Consider a captured video sequence with spatial resolution $H \times W$ pixels capturing the vibrating wire over a one second duration. Let $\mathbf{Y} \in \mathbb{R}^{m \times HW}$ denote the measured video frames from one second of video stacked into m rows, each consisting of the $H \times W$ pixels vectorized into a single row. We aim to recover a temporally super resolved video volume $\mathbf{U} \in \mathbb{R}^{N \times HW}$, where $N = cnm$, and the parameters c and n are as defined above.

Recall that every video frame indexed by i , or i th row of \mathbf{Y} , is captured through a coded illumination pattern \mathbf{a}_i during the frame exposure period. We can then form the measurement operator $\mathbf{A} \in \mathbb{R}^{m \times N}$ that relates the target high frame rate video \mathbf{U} to the measured video frames \mathbf{Y} using the following linear system:

$$\mathbf{Y} = \mathbf{A}\mathbf{U}. \tag{1}$$

Figure 1 shows an example measurement operator \mathbf{A} corresponding to the acquisition of five video frames. The illumination patterns \mathbf{a}_i are shown as the white lines in the figure. In this example, every frame exposure period is divided into five segments, where the first segment contains the illumination pattern. The remaining four segments correspond to the dead-time of the camera exposure.

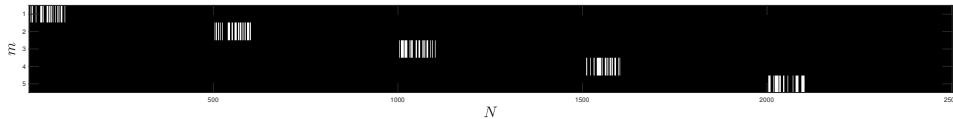


Figure 1: Example of the measurement operator \mathbf{A} for $m = 5$, $c = 5$, and $n = 100$. The white lines indicate instances when the strobing illumination is ON. In this example, every frame is observed through a different pseudorandom illumination pattern.

The effect of the measurement operator \mathbf{A} on a vibrating wire sequence can be perceived through the examples shown in Figures 2 and 3. The figures show a set of five video frames captured through the operator \mathbf{A} of an example vibrating sequence \mathbf{U} . The measurement operator results in blurring artifacts in the cases where the wire is moving. We append the mean of the observed video frames to the measurements as part of the measurement operator to help speed up the reconstruction of the DC component of the vibrating video.

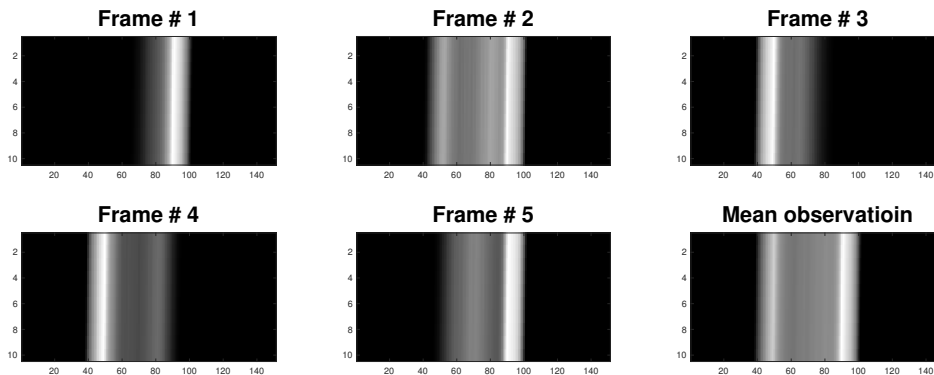


Figure 2: Example of the captured video frames from a vibrating wire where the measurements correspond to $m = 5$, $c = 5$, and $n = 100$. Every frame is composed of 10×151 pixels and the subplots illustrate the blurring effect resulting from observing the true vibrating wire through the measurement operator \mathbf{A} . The bottom right subplot corresponds to the mean of the five observed frames.

Notice from (1) that the operator \mathbf{A} acts on every pixel of the video in the same manner. As it stands, problem (1) is severely ill-posed since there we can find infinitely many solutions \mathbf{U} to the system of equation. However, since the wire is oscillating within a narrow frequency band, we may still be able to exactly reconstruct the true matrix \mathbf{U} by exploiting its sparsity in the frequency domain. Let $\mathbf{F} \in \mathbb{C}^{N \times N}$ be the N -dimensional *inverse* Fourier transform operator, and denote by $\mathbf{X} \in \mathbb{C}^{N \times HW}$ the frequency coefficient matrix of \mathbf{U} , i.e., $\mathbf{U} = \mathbf{F}\mathbf{X}$. Since any intensity fluctuation in the video is driven by the wire vibration, the

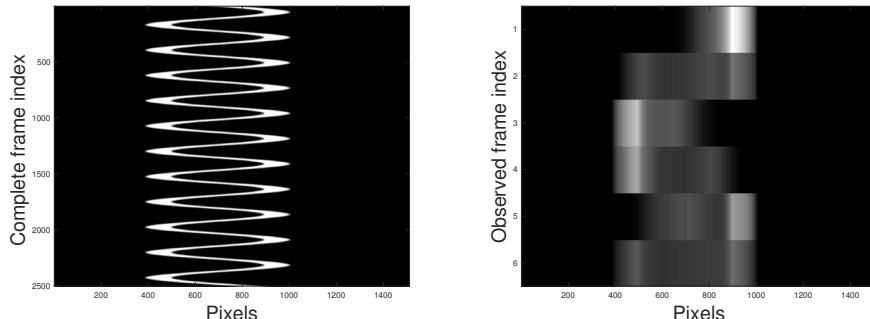


Figure 3: Example of the complete vibrating wire sequence \mathbf{U} compared to measured sequence \mathbf{Y} observed through the operator \mathbf{A} . The last row of \mathbf{Y} corresponds to the mean of the five observed frames.

locations of the significant nonzero coefficients in the columns of \mathbf{X} should fall within the same frequency bins. Consequently, we may exploit a jointly sparse structure in the matrix \mathbf{X} that allows us to leverage the multiple measurement vectors (columns of \mathbf{Y}) given by the different pixels in the observed video to recover the support of the row-norms of \mathbf{X} . One possible approach for employing the joint-sparsity prior on \mathbf{X} is to utilize an $\ell_{2,1}$ -norm penalty function and solve the following optimization problem:

$$\min_{\mathbf{X}} \frac{1}{2} \|\mathbf{Y} - \mathbf{A}\mathbf{F}\mathbf{X}\|_F^2 + \lambda \|\mathbf{X}\|_{2,1}, \quad (2)$$

where $\|\mathbf{X}\|_{2,1} = \sum_{r=1}^N \|\mathbf{X}(r, \cdot)\|_2$ and $\mathbf{X}(r, \cdot)$ denotes the r th row of \mathbf{X} .

In the context of sparse signal recovery, well established results in the field of compressed sensing have shown that a k -sparse vector of length N requires at least $2k + 1$ measurements to guarantee recovery [3, 4]. When multiple measurements are available, Chen and Huo [5, Theorem 2.4] showed that the necessary number of measurements can be reduced to $2k + 1 - \text{rank}(\mathbf{Y})$. Specifically, if a measurement matrix $\mathbf{Y} \in \mathbb{R}^{m,M}$ is not rank deficient, then the necessary number of measurements can be reduced by the $\min\{m, M\}$. This in turn implies that solving a joint sparsity problem does not benefit much from having multiple measurements M that are larger than m . We have conducted Monte Carlo simulations for joint sparsity reconstruction using $\ell_{2,1}$ minimization and observed that the simulations support our conjecture that the reconstruction quality does not improve much when $M > m$. On the other hand, the computational complexity increases significantly as M increases since the dimensionality of the optimization variable is $N \times M$.

3 Proposed Solution

We propose a framework where we first compress the dimensionality of problem (2) and identify the support of the jointly sparse signal \mathbf{X} . We then solve for coefficients of \mathbf{X} restricted to the identified support set in order to reconstruct the temporally super resolved video sequence.

3.1 Dimensionality reduction

One of the drawbacks of problem (2) is that it does not scale well with the number of pixels in each video frame since the optimization variable \mathbf{X} is $N \times HW$. However, following the argument presented in the previous paragraph, we see that there is no benefit to increasing the number of measurement vectors beyond the rank of \mathbf{Y} . Therefore, we propose to reduce the dimensionality of the problem by multiplying the measurements \mathbf{Y} from the right by a random matrix $\mathbf{B} \in \mathbb{R}^{HW \times m}$ to obtain the compressed data matrix

$$\begin{aligned} \tilde{\mathbf{Y}} &:= \mathbf{Y}\mathbf{B} \\ &= \mathbf{A}\mathbf{F}\mathbf{X}\mathbf{B} \\ &= \mathbf{A}\mathbf{F}\tilde{\mathbf{X}}. \end{aligned} \tag{3}$$

We note here that the support of the row norms of $\tilde{\mathbf{X}}$ is identical to that of \mathbf{X} . Using the compressed observation model in (3), we can now set up an equivalent $\ell_{2,1}$ -minimization problem to (2) as follows

$$\min_{\tilde{\mathbf{X}}} \frac{1}{2} \|\tilde{\mathbf{Y}} - \mathbf{A}\mathbf{F}\tilde{\mathbf{X}}\|_F^2 + \lambda \|\tilde{\mathbf{X}}\|_{2,1}, \tag{4}$$

which allows us to identify the support of \mathbf{X} while operating on a significantly lower dimensional optimization variable $\tilde{\mathbf{X}}$.

3.2 Support estimation

For solving (3), we adopt a modified FISTA algorithm [6] that is specialized for recovering row norm sparse signals as shown in Algorithm 1. In our modified FISTA routine, we first compute a quasi-Newton estimate $\hat{\mathbf{X}}$ for the variable $\tilde{\mathbf{X}}$ followed by the proximal mapping function $\mathbf{prox}_{\ell_{2,1}}(\hat{\mathbf{X}}; \alpha\lambda\bar{\mathbf{w}})$ with respect to a weighted $\ell_{2,1}$ norm of the estimate $\hat{\mathbf{X}}$ using the weight vector $\bar{\mathbf{w}}$ shown in Algorithm 1. The choice of the weight vector $\bar{\mathbf{w}} = 1 + 10|\mathbf{w}|/\|\mathbf{w}\|_\infty$, with $\mathbf{w} = \mathbf{F}^H\mathbf{A}^T\mathbf{1}$ is designed to discourage non-zero coefficients in the rows of \mathbf{X} that align with the sampling structure of the measurement operator \mathbf{A} .

The proximal mapping function is applied row-wise and is defined as follows for each row indexed by r :

$$\mathbf{prox}_{\ell_{2,1}}(\hat{\mathbf{X}}(r, :); \alpha\lambda\bar{\mathbf{w}}(r)) := \frac{\hat{\mathbf{X}}(r, :)}{\|\hat{\mathbf{X}}(r, :)\|_2} \cdot \max\left\{\|\hat{\mathbf{X}}(r, :)\|_2 - \alpha\lambda\bar{\mathbf{w}}(r), 0\right\}. \tag{5}$$

After computing $\tilde{\mathbf{X}}$ using Algorithm 1, we estimate the support set S of \mathbf{X} as the index set of the row-norm vector $\tilde{\mathbf{x}}$ of $\tilde{\mathbf{X}}$, i.e., the set of row indices that have non-zero ℓ_2 norms:

$$S = \text{supp}(\tilde{\mathbf{x}}), \text{ where } \tilde{\mathbf{x}} := \sqrt{\left(\tilde{\mathbf{X}} \odot \tilde{\mathbf{X}}^*\right) \mathbf{1}}, \quad (6)$$

where \odot denotes the element-wise Hadamard product, $\tilde{\mathbf{X}}^*$ is the element-wise complex conjugate of $\tilde{\mathbf{X}}$, and $\mathbf{1}$ is the all ones vector.

Algorithm 1 Modified `fista` subroutine for computing $\tilde{\mathbf{X}}$

input: $\mathbf{A}, \mathbf{F}, \tilde{\mathbf{Y}}, \lambda, T$.
set: $q_0 = 1, \mathbf{X}^0 = \mathbf{Z}^0 = \mathbf{0}$
1: $\alpha \leftarrow$ inverse of maximum eigenvalue of $\mathbf{F}^H \mathbf{A}^T \mathbf{A} \mathbf{F}$
2: $\mathbf{w} = \mathbf{F}^H \mathbf{A}^T \mathbf{1}$, $\bar{\mathbf{w}} = 1 + 10\|\mathbf{w}\|/\|\mathbf{w}\|_\infty$
3: $\mathbf{Q} \leftarrow \mathbf{F}^H \mathbf{A}^\dagger \mathbf{A}^{\dagger T} \mathbf{F}$, approximate inverse Hessian
4: **for** $t \leftarrow 1$ to T **do**
5: $\hat{\mathbf{X}}^t \leftarrow \mathbf{Z}^{t-1} + \mathbf{Q} \mathbf{F}^H \mathbf{A}^T \left(\tilde{\mathbf{Y}} - \mathbf{A} \mathbf{F} \mathbf{Z}^{t-1} \right)$
6: $\mathbf{X}^t \leftarrow \text{prox}_{\ell_{2,1}} \left(\hat{\mathbf{X}}^t; \alpha \lambda \bar{\mathbf{w}} \right)$
7: $q_t \leftarrow \frac{1 + \sqrt{1 + 4q_{t-1}^2}}{2}$
8: $\mathbf{Z}^t \leftarrow \mathbf{X}^t + \frac{q_{t-1} - 1}{q_t} (\mathbf{X}^t - \mathbf{X}^{t-1})$
return: $\tilde{\mathbf{X}} \leftarrow \mathbf{X}^T$

3.3 Video reconstruction

Once the support set S is identified, we reconstruct the high frame rate video $\mathbf{U} = \mathbf{F}_S \mathbf{X}_S$ by computing the coefficients of \mathbf{X} restricted to the support set S . The matrix \mathbf{F}_S is the subset of the columns of the inverse Fourier matrix indexed by S . This is achieved by solving the following constrained least squares problem:

$$\min_{\mathbf{X}_S} \frac{1}{2} \|\mathbf{Y} - \mathbf{A} \mathbf{F}_S \mathbf{X}_S\|_F^2 \text{ subject to } \mathbf{F}_S \mathbf{X}_S \geq 0. \quad (7)$$

The constraint $\mathbf{F}_S \mathbf{X}_S \geq 0$ above ensures that every pixel in $\mathbf{U} \in \mathbb{R}_+$ has a real, non-negative feasible pixel value. Problem (7) can be solved using an accelerated projected gradient (APG) descent routine shown in Algorithm 2. The constraint of \mathbf{U} to the positive orthant is guaranteed through the element-wise projection operator $\text{proj}_{\mathbb{R}_+}(\mathbf{U})$ that discards the imaginary component of every element of \mathbf{U} and sets any negative real component to zero.

3.4 Outlier robustness

In practical EDM scenarios, the wire vibrates inside of an injected fluid that helps in lubricating and cooling the mechanical components. The presence of

Algorithm 2 Accelerated projected gradient (APG) routine for computing \mathbf{U} .

input: $\mathbf{A}, \mathbf{F}_S, \mathbf{Y}, T$.
set: $q_0 = 1, \mathbf{X}_S^0 = \mathbf{Z}^0 = \mathbf{0}$
1: $\alpha \leftarrow$ inverse of maximum eigenvalue of $\mathbf{F}_S^H \mathbf{A}^T \mathbf{A} \mathbf{F}_S$
2: **for** $t \leftarrow 1$ to T **do**
3: $\hat{\mathbf{X}}_S^t \leftarrow \mathbf{Z}^{t-1} + \alpha \mathbf{F}_S^H \mathbf{A}^T (\mathbf{Y} - \mathbf{A} \mathbf{F}_S \mathbf{Z}^{t-1})$
4: $\mathbf{U}^t \leftarrow \text{proj}_{\mathbb{R}_+} (\mathbf{F}_S \hat{\mathbf{X}}_S^t)$
5: $\mathbf{X}_S^t \leftarrow \mathbf{F}_S^H \mathbf{U}^t$
6: $q_t \leftarrow \frac{1 + \sqrt{1 + 4q_{t-1}^2}}{2}$
7: $\mathbf{Z}^t \leftarrow \mathbf{X}_S^t + \frac{q_{t-1} - 1}{q_t} (\mathbf{X}_S^t - \mathbf{X}_S^{t-1})$
return: $\mathbf{U} \leftarrow \mathbf{U}^T$

the fluid and the wire vibration often result in the occurrence of air bubbles that move through the fluid. These bubbles are captured by the video camera and their motion induces spectral components that contaminate the spectrum of a purely vibrating wire. Fortunately, the motion of the bubbles is not periodic and the occurrence of the bubbles in the captured video is generally transient.

Given the above properties of the bubbles, we propose to model the presence of the bubbles as sparse outliers in the measurement model. To be precise, let $\mathbf{O} \in \mathbb{R}^{m \times HW}$ denote the sparse matrix of outliers corresponding to the bubbles. The new forward model that accommodates the presence of bubbles is given by:

$$\mathbf{Y} = \mathbf{A} \mathbf{F} \mathbf{X} + \mathbf{O}. \quad (8)$$

Since our goal is to recover \mathbf{X} and its support, we need to develop a mechanism for handling the presence of the sparse outlier matrix \mathbf{O} . Below we propose two formulations that address this task.

3.4.1 Bubble separation using robust PCA

The sparsity of the row norms of \mathbf{X} result in the matrix $\mathbf{L} := \mathbf{A} \mathbf{F} \mathbf{X}$ to have a low rank. One commonly used technique for separating the sum of a low rank component and a sparse component is robust principal component analysis (PCA). The robust PCA problem can be summarized as follows:

$$\min_{\mathbf{L}, \mathbf{O}} \|\mathbf{L}\|_* + \|\mathbf{O}\|_1 \text{ subject to } \mathbf{Y} = \mathbf{L} + \mathbf{O}, \quad (9)$$

where $\|\mathbf{L}\|_*$ denotes the nuclear norm (sum of singular values) of a matrix \mathbf{L} , and $\|\mathbf{O}\|_1$ is the ℓ_1 norm of the vectorized matrix \mathbf{O} .

With this approach, we first solve the robust PCA problem to compute the low rank matrix \mathbf{L} , and then proceed with our support estimation and video reconstruction steps described above after replacing the matrix \mathbf{Y} with the low rank matrix \mathbf{L} .

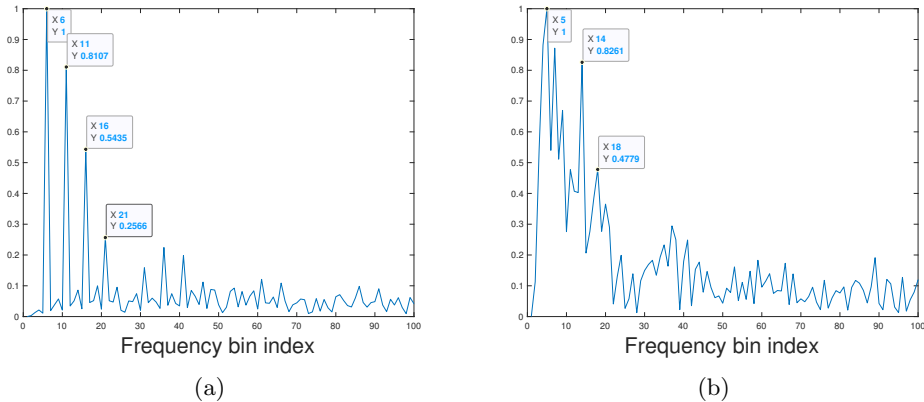


Figure 4: Plots of the magnitudes of the spectrum signal $\mathbf{w} = \mathbf{F}^H \mathbf{A}^T \mathbf{1}$ for (a) the uniform sampling operator, and (b) the random sampling operator.

3.4.2 Bubble separation through forward modeling

As an alternative to the robust PCA approach, we may incorporate the bubble separation stage directly into the support identification step from compressed measurements shown in (10) above. Specifically, we rewrite (10) as follows:

$$\min_{\tilde{\mathbf{X}}, \mathbf{O}} \frac{1}{2} \|\tilde{\mathbf{Y}} - \mathbf{A}\tilde{\mathbf{F}}\tilde{\mathbf{X}} - \mathbf{O}\mathbf{B}\|_F^2 + \lambda \|\tilde{\mathbf{X}}\|_{2,1} + \mu \|\mathbf{O}\|_1, \quad (10)$$

where we recall that \mathbf{B} is the dimensionality reducing random matrix.

4 Sensing System Design

The design of the sensing matrix \mathbf{A} plays an important role in determining the reconstruction quality of the super resolved video. Particularly, the instantiation and length of the coded illumination pattern within a video frame exposure period can impact the ability to determine the correct signal support. Recall that our target is to identify the frequency (or sparse support set of frequencies) of a period signal \mathbf{U} . If the coded illumination patterns \mathbf{a}_i are triggered at uniformly spaced intervals, then the operator \mathbf{A} also exhibits a sparse spectrum in the frequency domain, which may not be distinguishable from the support of the signal \mathbf{U} . We observe this behavior by plotting the spectrum signal $\mathbf{w} = \mathbf{F}^H \mathbf{A}^T \mathbf{1}$ in Figure 4(a) for the example sampling operator shown in Figure 5(a). We can see from the figure that the frequency corresponding to the video frame rate m and its harmonics are the dominating coefficients.

Alternatively, we may allow the strobing sequence occupy a random starting position in the frame exposure interval as shown in Figure 5(b). This approach helps in breaking the periodicity of the sampling operator and results in a rel-

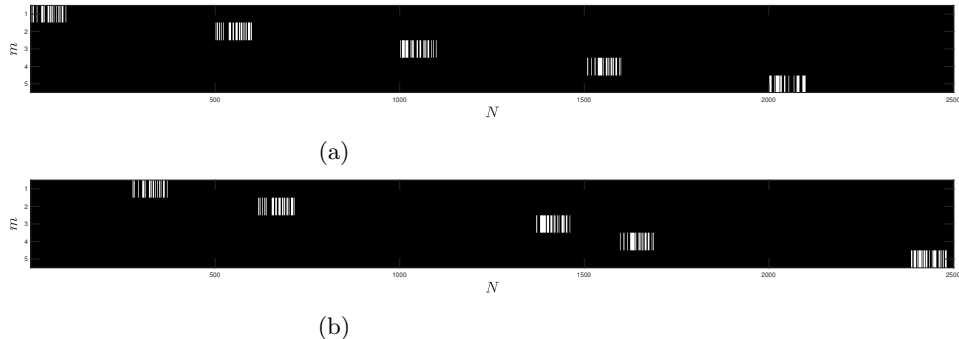


Figure 5: Illustration of (a) the uniform sampling operator with strobing sequences starting at the beginning of the frame exposure interval, and (b) the random sampling operator where the strobing sequence can begin at any point in the frame interval.

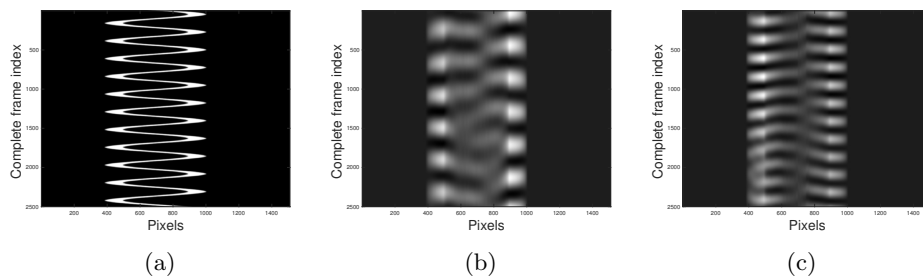


Figure 6: (a) High temporal resolution ground truth video and the reconstructed video from (b) the uniform sampling operator and (c) the randomized sampling operator.

atively *flatter* spectrum that does not exhibit the high valued coefficients at harmonic frequencies as can be seen from Figure 4(b).

5 Numerical Evaluation

We evaluated the performance of our proposed scheme with an example video sequence of a wire vibrating at 11 Hz. We limit the experiment to such low a frequency in order to help with the visualizations. The video camera captures frames at $m = 5$ Hz and the strobing sequence has a duration of 40 ms with $n = 100$ being the length of each strobing code \mathbf{a}_i . Consequently, the target temporal resolution time step $t_s = 0.4$ ms and the temporal dimension of the super resolved sequence is $N = 2500$, i.e., a $500\times$ super resolution rate. The experimental parameters described here correspond to the setup shown in Figure 2.

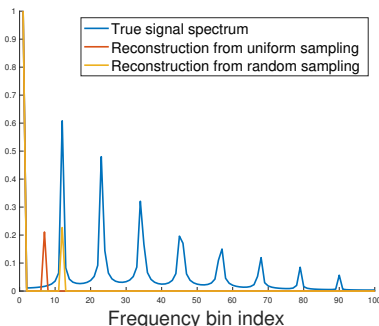


Figure 7: Comparison of the Fourier coefficients of the ground truth and the reconstructed videos from the uniform and randomized sampling operators.

We restrict the experiment to the bubble free setup and follow the procedure described in this note to reconstruct the temporally super resolved video frames. Figure 6 compares the reconstructed video quality between the uniform sensing operator and the randomized operator. It is evident from the result that the randomized operator shows better reconstruction compared to the uniform operator. We caution though that this is a particular adversarial example for the uniform sampling operator. Moreover, the randomization seed has a significant effect on the ability to reconstruct the true support, i.e., not every randomization is capable of capturing the correct support.

References

- [1] P. Boufounos and M. S. Asif, “Compressive sampling for streaming signals with sparse frequency content,” in *2010 44th Annual Conference on Information Sciences and Systems (CISS)*, 2010, pp. 1–6.
- [2] A. Veeraraghavan, D. Reddy, and R. Raskar, “Coded strobing photography: Compressive sensing of high speed periodic videos,” *IEEE Transactions on Pattern Analysis and Machine Intelligence*, vol. 33, no. 4, pp. 671–686, 2011.
- [3] D. Donoho, “Compressed sensing,” *IEEE Transactions on Information Theory*, vol. 52, no. 4, pp. 1289–1306, 2006.
- [4] E. J. Candès, J. Romberg, and T. Tao, “Stable signal recovery from incomplete and inaccurate measurements,” *Communications on Pure and Applied Mathematics*, vol. 59, pp. 1207–1223, 2006.
- [5] J. Chen and X. Huo, “Theoretical results on sparse representations of multiple-measurement vectors,” *IEEE Transactions on Signal Processing*, vol. 54, no. 12, pp. 4634–4643, 2006.

- [6] Amir Beck and Marc Teboulle, “A fast iterative shrinkage-thresholding algorithm for linear inverse problems,” *SIAM Journal on Imaging Sciences*, vol. 2, no. 1, pp. 183–202, 2009.